

## Enhancement of oxygen surface exchange on epitaxial $\text{La}_{0.6}\text{Sr}_{0.4}\text{Co}_{0.2}\text{Fe}_{0.8}\text{O}_{3-\delta}$ thin films using advanced heterostructured oxide interface engineering

**Dongkyu Lee**, Electrochemical Energy Laboratory, Massachusetts Institute of Technology, 77 Massachusetts Avenue, Cambridge, MA 02139, USA; Department of Mechanical Engineering, Massachusetts Institute of Technology, 77 MA Avenue, Cambridge, MA 02139, USA; Materials Science and Technology Division, Oak Ridge National Laboratory, Oak Ridge, TN 37831, USA

**Yueh-Lin Lee**, and **Xiao Renshaw Wang**, Electrochemical Energy Laboratory, Massachusetts Institute of Technology, 77 Massachusetts Avenue, Cambridge, MA 02139, USA; Department of Mechanical Engineering, Massachusetts Institute of Technology, 77 MA Avenue, Cambridge, MA 02139, USA

**Dane Morgan**, Department of Materials Science and Engineering, University of Wisconsin–Madison, 1509 University Avenue, Madison, WI 53706, USA

**Yang Shao-Horn**, Electrochemical Energy Laboratory, Massachusetts Institute of Technology, 77 Massachusetts Avenue, Cambridge, MA 02139, USA; Department of Mechanical Engineering, Massachusetts Institute of Technology, 77 MA Avenue, Cambridge, MA 02139, USA; Department of Materials Science and Engineering, Massachusetts Institute of Technology, 77 Massachusetts Avenue, Cambridge, MA 02139, USA

Address all correspondence to Yang Shao-Horn at [shaohorn@mit.edu](mailto:shaohorn@mit.edu)

(Received 8 May 2016; accepted 2 August 2016)

### Abstract

Engineering of a novel heterostructured oxide interface was used to enhance the oxygen surface exchange kinetics of  $\text{La}_{0.6}\text{Sr}_{0.4}\text{Co}_{0.2}\text{Fe}_{0.8}\text{O}_{3-\delta}$  (LSCF<sub>113</sub>) thin films. A single-layer decoration of mixed  $(\text{LaSr})_2\text{CoO}_{4\pm\delta}$  (LSC<sub>214</sub>) and  $\text{La}_{1-x}\text{Sr}_x\text{CoO}_{3-\delta}$  (LSC<sub>113</sub>) and a double-layer decoration of stacked LSC<sub>214</sub> and LSC<sub>113</sub> grown on the LSCF<sub>113</sub> markedly enhanced the surface exchange coefficients of the LSCF<sub>113</sub> by up to ~1.5 orders of magnitude relative to the undecorated LSCF<sub>113</sub>. It is hypothesized that two different types of surface decorations can enable Sr segregation at the interface and surfaces of LSC<sub>113</sub> and LSC<sub>214</sub>, leading to enhancement of the oxygen surface exchange kinetics of decorated LSCF<sub>113</sub>.

The development of highly active cathode materials is essential to lower the operating temperature of solid oxide fuel cells (SOFCs), where the slow kinetics of the oxygen surface exchange on the cathode surface limits the efficiency of SOFCs at intermediate temperatures (500–750 °C).<sup>[1,2]</sup> Current cathode materials such as  $\text{La}_{1-x}\text{Sr}_x\text{MnO}_{3-\delta}$  (LSM<sub>113</sub>)<sup>[3–5]</sup> with high electronic conductivity but low ionic conductivity<sup>[6]</sup> are inadequate for the usage in the intermediate temperature range due to insufficient surface activity.

$\text{La}_{1-x}\text{Sr}_x\text{Fe}_{1-y}\text{Co}_y\text{O}_{3-\delta}$  (LSCF<sub>113</sub>), which has beneficial materials properties such as high ionic and electronic conductivity,<sup>[7]</sup> and fast oxygen surface exchange,<sup>[8]</sup> therefore, has been developed as one of the most promising commercial cathode materials for intermediate temperature SOFCs. In particular, a solution infiltration process, in which a phase transition occurs from a liquid into a solid has been widely used to further enhance the surface activity of LSCF<sub>113</sub>.<sup>[9–12]</sup> Utilizing infiltrated LSM<sub>113</sub> coatings, it has been shown the enhanced electrocatalytic activity of LSCF<sub>113</sub> cathodes.<sup>[11,12]</sup> Infiltrated  $\text{La}_{0.4875}\text{Ca}_{0.0125}\text{Ce}_{0.5}\text{O}_{2-\delta}$  (LCC)<sup>[9]</sup> and  $\text{Sm}_{0.5}\text{Sr}_{0.5}\text{CoO}_{3-\delta}$  (SSC)<sup>[10]</sup> coatings have also been used for better stability and activity of LSCF<sub>113</sub> electrodes. Although many studies have shown the enhanced cathodic performance of LSCF<sub>113</sub> by surface modification through a solution-based infiltration process,

the origin responsible for the enhanced stability and activity of decorated LSCF<sub>113</sub> cathode is poorly understood.

Ruddlesden-Popper (RP) phases ( $A_2\text{BO}_4$ ) have been utilized as a material for the  $\text{La}_{1-x}\text{Sr}_x\text{CoO}_{3-\delta}$  (LSC<sub>113</sub>) surface modification, which results in the enhanced surface activity of LSC<sub>113</sub> significantly due to the formation of heterostructured oxide interfaces.<sup>[13–18]</sup> Using well-defined epitaxial thin film systems, remarkably enhanced oxygen surface exchange kinetics (up to ~2 orders of magnitude) of LSC<sub>113</sub> has been reported by decorating  $(\text{La}_{0.5}\text{Sr}_{0.5})_2\text{CoO}_{4\pm\delta}$  (LSC<sub>214</sub>) phase on the LSC<sub>113</sub> surface.<sup>[13,19]</sup> Coherent Bragg rod analysis (COBRA) and density functional theory (DFT) have suggested that the enhanced oxygen surface exchange kinetics may be attributed to the Sr segregation at the LSC<sub>214</sub>–LSC<sub>113</sub> interface and the LSC<sub>214</sub> surface, resulting from a large driving force for A-site cation interdiffusion across the heterostructured interface.<sup>[14,15,20]</sup> In addition, the enhanced activity of LSC<sub>113</sub> may also be attributed to the stabilized LSC<sub>113</sub> surface by LSC<sub>214</sub> phase, which suppresses the formation of Sr-enriched secondary particles on the LSC<sub>113</sub> surface after a long-time annealing.<sup>[17]</sup> However, the heterostructured oxide interfaces formed by decorating LSC<sub>214</sub> on LSCF<sub>113</sub> perovskites have shown negligible enhancement (up to two times) of the oxygen surface exchange kinetics of LSCF<sub>113</sub>,<sup>[17]</sup> which can be attributed to no further

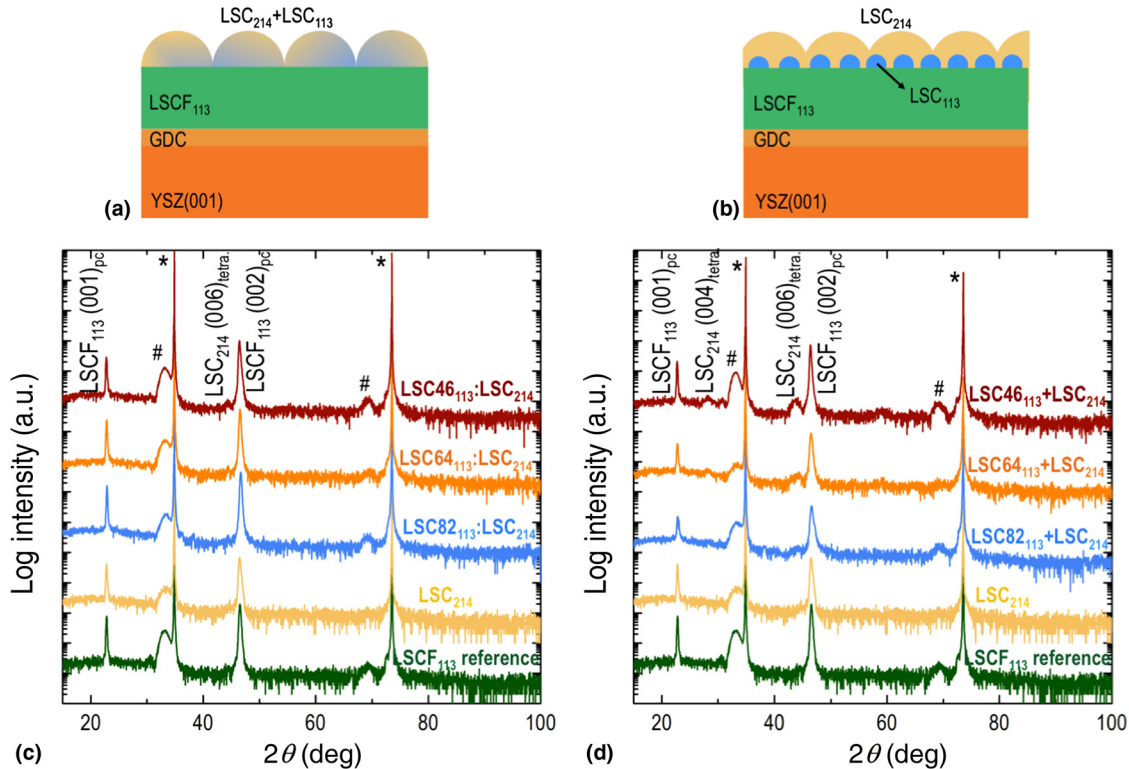


**Figure 1.** Schematic representation of (a) the  $\text{LSCF}_{113}$  with single-layer decoration of mixed  $\text{LSC}_{214}$  and  $\text{LSC}_{113}$ , and (b) with double-layer decoration of stacked  $\text{LSC}_{214}$  and  $\text{LSC}_{113}$  epitaxial thin films. High-resolution XRD analysis of (c) the  $\sim 65$  nm  $\text{LSCF}_{113}$  reference (green), the  $\sim 3$  nm  $\text{LSC}_{214}$ -decorated  $\text{LSCF}_{113}$  (yellow), and the  $\text{LSCF}_{113}$  with  $\sim 3$  nm single-layer decorations of mixed  $\text{LSC}_{214}$  and  $\text{LSC}_{82113}$  (blue),  $\text{LSC}_{64113}$  (orange), and  $\text{LSC}_{46113}$  (red), and (d) the  $\sim 65$  nm  $\text{LSCF}_{113}$  reference (green), the  $\sim 3$  nm  $\text{LSC}_{214}$ -decorated  $\text{LSCF}_{113}$  (yellow), and the  $\text{LSCF}_{113}$  with double-layer decorations of stacked  $\sim 3$  nm  $\text{LSC}_{214}$  and  $\sim 0.5$  nm  $\text{LSC}_{82113}$  (blue),  $\sim 0.5$  nm  $\text{LSC}_{64113}$  (orange), and  $\sim 0.5$  nm  $\text{LSC}_{46113}$  (red) epitaxial thin films on (001) YSZ substrates with GDC buffer layer. YSZ substrate and GDC peaks are indicated with pounds (#) and asterisks (\*), respectively.

increase in Sr concentration at the surface of  $\text{LSCF}_{113}$  induced by  $\text{LSC}_{214}$  decoration. While growing a more Sr-rich  $\text{LSC}_{214}$  on  $\text{LSCF}_{113}$  might yield enhancement due to the high oxygen surface exchange kinetics of  $\text{LSC}_{214}$  ( $x_{\text{Sr}} > 1.0$ ),<sup>[15,21]</sup> such an approach is inhibited by difficulties in the synthesis of RP phase with high Sr substitution.<sup>[22,23]</sup>

In this study, we have developed the heterostructured oxide decoration on  $\text{LSCF}_{113}$ , which leads to the enhancement of the surface activity of the  $\text{LSCF}_{113}$ . Utilizing pulsed laser deposition (PLD), we employ two different types of surface decorations on the epitaxial  $\text{LSCF}_{113}$  thin films, which are the single-layer decoration of mixed  $\text{LSC}_{214}$  and  $\text{LSC}_{113}$  and the double-layer decoration of stacked  $\text{LSC}_{214}$  and  $\text{LSC}_{113}$ . These structures stabilize the  $\text{LSC}_{113}$  phase, providing sufficient Sr sources and thermodynamic driving force for the Sr interdiffusion between  $\text{LSC}_{214}$  and  $\text{LSC}_{113}$ . Electrochemical impedance spectroscopy (EIS) study reveals that the oxygen surface exchange coefficients ( $k^j$ ) of the  $\text{LSCF}_{113}$  thin films can be significantly enhanced up to  $\sim 1.5$  orders of magnitudes higher than those of the undecorated  $\text{LSCF}_{113}$  by the heterostructured oxide interface engineering. In addition, the  $\text{LSC}_{113}$  with higher Sr content relative to the  $\text{LSC}_{214}$  single

phase in both single-layer and double-layer decoration leads to higher enhancement in the surface exchange kinetics of the  $\text{LSCF}_{113}$ , which suggests that the enhancement of the surface exchange kinetics of the  $\text{LSCF}_{113}$  can be attributed to an increase of Sr concentration on the multiphase heterostructured interface.

PLD was used to deposit the epitaxial  $\sim 65$  nm  $\text{LSCF}_{113}$  thin films with the  $\sim 3$  nm single-layer decoration of mixed  $\text{LSC}_{214}$  and  $\text{LSC}_{113}$  [Fig. 1(a)] and the double-layer decoration of stacked  $\sim 3$  nm  $\text{LSC}_{214}$  and  $\sim 0.5$  nm  $\text{LSC}_{113}$  [Fig. 1(b)] on an yttria-stabilized zirconia (YSZ) (001) substrate with a Gd-doped ceria (GDC) buffer layer. Out-of-plane x-ray diffraction (XRD) results [Figs. 1(c) and 1(d)] of the undecorated  $\text{LSCF}_{113}$ ,  $\text{LSC}_{214}$ -decorated  $\text{LSCF}_{113}$ , the  $\text{LSCF}_{113}$  with the single-layer decoration of mixed  $\text{LSC}_{214}$  and  $\text{LSC}_{113}$  thin films, and the  $\text{LSCF}_{113}$  with the double-layer decoration of stacked  $\text{LSC}_{214}$  and  $\text{LSC}_{113}$  thin films clearly show the presence of the  $(00l)_{\text{pc}}$  ( $l$  is integer) peaks of  $\text{LSCF}_{113}$  and  $(00l)_{\text{cubic}}$  ( $l$  is even) peaks of GDC and YSZ, indicating that the  $\text{LSCF}_{113}$  film was grown epitaxially with the following epitaxial relationships:  $(001)_{\text{pc}}\text{LSCF}_{113} // (001)_{\text{cubic}}\text{GDC} // (001)_{\text{cubic}}\text{YSZ}$  (where “pc” denotes the pseudocubic notation).

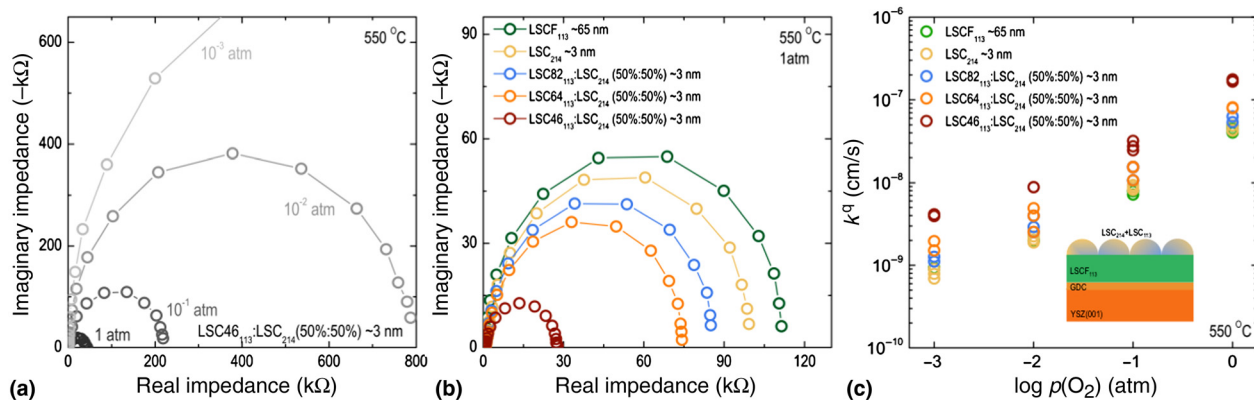


**Figure 2.** EIS results of microelectrodes (200  $\mu\text{m}$  in diameter) for the epitaxial  $\text{LSCF}_{113}$  thin films with  $\text{LSC}_{214}$  decoration, and single-layer decorations of mixed  $\text{LSC}_{214}$  and  $\text{LSC}_{113}$  on  $\text{YSZ}$  (001) with a GDC buffer layer at 550  $^{\circ}\text{C}$ . (a) Nyquist plot at 550  $^{\circ}\text{C}$  as a function of oxygen partial pressure,  $p(\text{O}_2)$ , of the  $\text{LSCF}_{113}$  thin films with single-layer decoration of mixed  $\text{LSC}_{214}$  and  $\text{LSC}_{46113}$ . (b) Nyquist plot at 550  $^{\circ}\text{C}$  with an 1 atm of  $p(\text{O}_2)$  of the  $\text{LSCF}_{113}$  (green), the  $\text{LSC}_{214}$ -decorated  $\text{LSCF}_{113}$  (yellow), and the  $\text{LSCF}_{113}$  with  $\sim 3$  nm single-layer decoration of mixed  $\text{LSC}_{214}$  and  $\text{LSC}_{82113}$  (blue),  $\text{LSC}_{64113}$  (orange), and  $\text{LSC}_{46113}$  (red) thin films. (c)  $p(\text{O}_2)$  dependency of the surface exchange coefficients ( $k^l$ ) of the  $\text{LSCF}_{113}$  (green), the  $\text{LSC}_{214}$ -decorated  $\text{LSCF}_{113}$  (yellow), and the  $\text{LSCF}_{113}$  with  $\sim 3$  nm single-layer decoration of mixed  $\text{LSC}_{214}$  and  $\text{LSC}_{82113}$  (blue),  $\text{LSC}_{64113}$  (orange), and  $\text{LSC}_{46113}$  (red) thin films. All EIS spectra were collected at 550  $^{\circ}\text{C}$ .

With higher Sr content of  $\text{LSC}_{113}$  in the single- and double-layer decorations, the  $(00l)_{\text{tetra}}$  ( $l$  is the integer) peaks of  $\text{LSC}_{214}$  become visible, which represents  $(001)_{\text{tetra}}.\text{LSC}_{214} // (001)_{\text{pc}}.\text{LSCF}_{113} // (001)_{\text{cubic}}.\text{GDC} // (001)_{\text{cubic}}.\text{YSZ}$ . The subscript “tetra.” denotes the tetragonal notation.<sup>[24,25]</sup> Off-normal phi-scan analysis of the undecorated  $\text{LSCF}_{113}$  and  $\text{LSC}_{214}$ -decorated  $\text{LSCF}_{113}$  films shows that  $\text{LSC}_{214} \{103\}_{\text{tetra}}$ ,  $\text{LSCF}_{113} \{202\}_{\text{pc}}$ ,  $\text{GDC} \{202\}_{\text{cubic}}$ , and  $\text{YSZ} \{202\}_{\text{cubic}}$  have strong peaks with fourfold cubic symmetry (Fig. S1†). This reveals the in-plane crystallographic relationships between GDC and YSZ (a cube-on-cube alignment),  $\text{LSCF}_{113}$  and GDC (an in-plane  $45^{\circ}$  rotation with  $[100]_{\text{pc}}.\text{LSCF}_{113} // [110]_{\text{cubic}}.\text{GDC} // [110]_{\text{cubic}}.\text{YSZ}$ ), and  $\text{LSCF}_{113}$  and  $\text{LSC}_{214}$  (no rotation with  $[100]_{\text{pc}}.\text{LSCF}_{113} // [100]_{\text{tetra}}.\text{LSC}_{214}$ ). Similar to our previous studies,<sup>[13,14,17,19]</sup> the relaxed lattice parameters,  $\hat{a}$  of the epitaxial  $\text{LSCF}_{113}$  films with and without surface decoration in this study at room temperature did not change significantly, ranging from 3.898–3.904  $\text{\AA}$  (Table S1†). As shown in Table S1†, both in-plane and out-of-plane strains of  $\text{LSCF}_{113}$  films were not strongly influenced by the surface decoration, which is supported by the fact that the lattice constant of  $\text{LSC}_{214}$  ( $a_{\text{tetra}} \approx 3.819$   $\text{\AA}$  for  $\text{LSC}_{214}$  bulk<sup>[26]</sup>) is very close to that of  $\text{LSCF}_{113}$  ( $a_{\text{pc}} \approx 3.885$   $\text{\AA}$  for the  $\text{LSCF}_{113}$  bulk<sup>[27]</sup>) and  $\text{LSC}_{113}$  ( $a_{\text{pc}} \approx 3.854$   $\text{\AA}$  for the  $\text{LSC}_{113}$  bulk<sup>[28]</sup>). This observation is further supported by our recent work,<sup>[14]</sup> where the  $\text{LSC}_{214}$  decoration has no influence on the in-plane and out-of-plane strains of the epitaxial  $\text{LSC}_{113}$  films at elevated temperatures. Details about deposition, lattice parameter calculation, and high-resolution XRD of  $\text{LSC}_{214}$ -decorated  $\text{LSC}_{113}$  film can be found in the ESI†.

EIS results of geometrically well-defined microelectrodes (200  $\mu\text{m}$  in diameter), measured at 550  $^{\circ}\text{C}$  are shown in Fig. 2. These microelectrodes were fabricated by photolithography and acid etched for the epitaxial  $\text{LSCF}_{113}$  thin films with

$\text{LSC}_{214}$  decoration and single-layer decorations of mixed  $\text{LSC}_{214}$  and three different Sr contents of  $\text{LSC}_{113}$  (Sr = 0.2, 0.4, and 0.6). The predominant semicircle was found to increase with decreasing oxygen partial pressure [Fig. 2(a)], where EIS data of all samples used in this study showed nearly perfect semicircle impedances.<sup>[6]</sup> Considering the fact that the film thicknesses are much smaller than the critical thickness for bulk transport limitation (estimated to 3.28  $\mu\text{m}$  for bulk  $\text{LSCF}_{113}$  at 550  $^{\circ}\text{C}$ <sup>[29]</sup>), the oxygen partial pressure [ $p(\text{O}_2)$ ]-dependent impedance responses suggest that the oxygen surface exchange kinetics governs the oxygen electrocatalysis on the film surface. In Fig. 2(b), the real part of the impedance of the predominant semicircle decreased with increasing Sr content of  $\text{LSC}_{113}$  in the single-layer decoration of mixed  $\text{LSC}_{214}$  and  $\text{LSC}_{113}$ , where the oxygen surface exchange coefficient ( $k^l$ ) of the  $\text{LSCF}_{113}$  with mixed  $\text{LSC}_{214}$  and  $\text{La}_{0.4}\text{Sr}_{0.6}\text{CoO}_{3-\delta}$  ( $\text{LSC}_{46113}$ ) decoration was found to be  $\sim 7$  times higher than that of undecorated  $\text{LSCF}_{113}$  and  $\text{LSC}_{214}$ -decorated  $\text{LSCF}_{113}$ . This observation indicates that higher Sr content in mixed  $\text{LSC}_{214}$  and  $\text{LSC}_{113}$  decoration can lead to higher surface exchange kinetics of the  $\text{LSCF}_{113}$ .

To further investigate the effect of Sr concentration in the mixed  $\text{LSC}_{214}$  and  $\text{LSC}_{113}$  phase on the surface exchange kinetics of the  $\text{LSCF}_{113}$ , a different ratio between  $\text{LSC}_{214}$  and  $\text{LSC}_{46113}$  was applied for decorating the surface of the  $\text{LSCF}_{113}$ . EIS data collected from the  $\text{LSCF}_{113}$  with and without the single-layer decoration of mixed  $\text{LSC}_{214}$  and  $\text{LSC}_{46113}$  thin films at 550  $^{\circ}\text{C}$  with an  $p(\text{O}_2)$  of 1 atm is shown in Fig. 3 (a). It is noted that the  $k^l$  values of the  $\text{LSCF}_{113}$  with 75% of  $\text{LSC}_{214}$  and 25% of  $\text{LSC}_{46113}$  decoration were found to be  $\sim 1.1$  orders of magnitude higher than those of the  $\text{LSCF}_{113}$  with and without  $\text{LSC}_{214}$  decoration, as shown in Fig. 3(b). To understand these changes we consider if the decorations may lead to the enhancement of Sr in the  $\text{LSCF}_{113}$  surface,

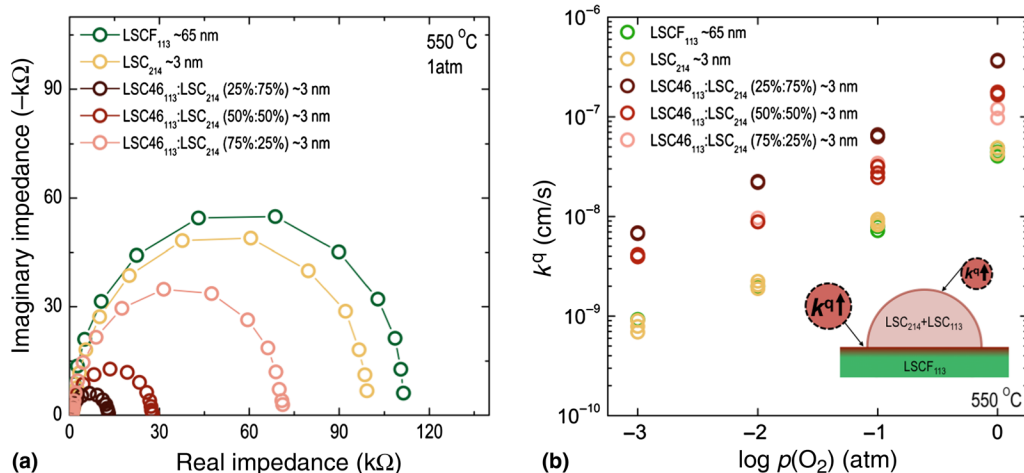


**Figure 3.** EIS results of microelectrodes (200  $\mu\text{m}$  in diameter) for the epitaxial LSCF<sub>113</sub> thin films with LSC<sub>214</sub> decoration, and single-layer decorations of mixed LSC<sub>214</sub> and LSC46<sub>113</sub> on YSZ (001) with a GDC buffer layer at 550 °C. (a) Nyquist plot at 550 °C with an 1 atm of  $p(\text{O}_2)$  of the LSCF<sub>113</sub> (green), the LSC<sub>214</sub>-decorated LSCF<sub>113</sub> (yellow), and the LSCF<sub>113</sub> with  $\sim 3$  nm single-layer decoration of mixed LSC<sub>214</sub> and LSC64<sub>113</sub> (75%:25%) (dark red), LSC<sub>214</sub> and LSC64<sub>113</sub> (50%:50%) (red), and LSC<sub>214</sub> and LSC64<sub>113</sub> (25%:75%) (light red) thin films. (b)  $p(\text{O}_2)$  dependency of  $k^q$  calculated from EIS spectra collected at 550 °C of the LSCF<sub>113</sub> (green), the LSC<sub>214</sub>-decorated LSCF<sub>113</sub> (yellow), and the LSCF<sub>113</sub> with  $\sim 3$  nm single-layer decoration of mixed LSC<sub>214</sub> and LSC64<sub>113</sub> (75%:25%) (dark red), LSC<sub>214</sub> and LSC64<sub>113</sub> (50%:50%) (red), and LSC<sub>214</sub> and LSC64<sub>113</sub> (25%:75%) (light red) thin films. Inset shows a hypothetical model: enhancement of the Sr content at the top surface of the LSCF<sub>113</sub> due to adding LSC<sub>113</sub> to LSC<sub>214</sub>.

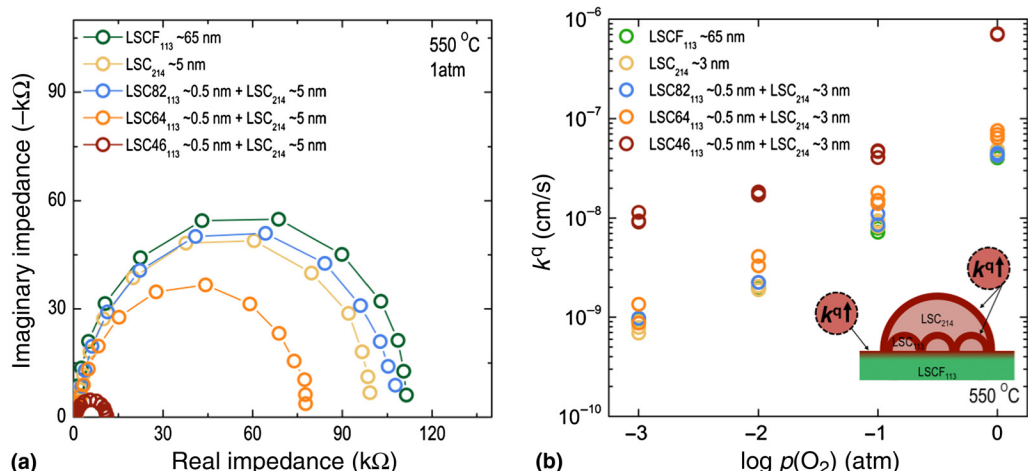
which would be expected to increase the oxygen  $2p$  band center relative to the Fermi level,<sup>[17]</sup> which in turn is expected to correlate with the enhancement of the oxygen surface exchange kinetics.<sup>[17,20,30]</sup> In the case of the LSC<sub>214</sub> decorated LSCF<sub>113</sub>, it has been proposed that low enhancement is observed because there is a negligible change of the surface Sr concentration at the heterostructured interface due to the initially high Sr surface concentration ( $\sim 100\%$ ) of the stable LSCF<sub>113</sub> (001) surface. This high Sr concentration cannot be easily increased. In contrast, the addition of the LSC<sub>113</sub> phase into the LSC<sub>214</sub> can provide the increased Sr content in LSC<sub>214</sub> and associated thermodynamic driving force for Sr interdiffusion from the LSC<sub>113</sub> into the LSC<sub>214</sub>. We propose that this driving force is large enough to result in higher Sr concentration in the surface decoration layer of mixed LSC<sub>214</sub> and LSC<sub>113</sub> on the LSCF<sub>113</sub> surface. Accordingly, this Sr enrichment is expected to uplift the oxygen  $2p$  band center (relative to the Fermi level) of the LSCF<sub>113</sub> interface layer and enhance the oxygen exchange kinetics of the LSCF<sub>113</sub>, as reported previously.<sup>[17]</sup> Interestingly, the enhancement in the surface exchange kinetics of the LSCF<sub>113</sub> was found to decrease with increasing the LSC46<sub>113</sub> ratio in the LSC<sub>214</sub> phase. This can be explained by the fact that the LSC<sub>214</sub> phase becomes unstable with increasing LSC46<sub>113</sub>, which can be supported by the reduced intensity of LSC<sub>214</sub> (001)<sub>tetra</sub> peak in Fig. S2†. Although a detailed study of the electronic structure changes is needed, the enhanced Sr concentration in the LSC<sub>214</sub> by mixing with LSC<sub>113</sub> may be responsible for enhancing the surface exchange kinetics of the LSCF<sub>113</sub>.

Figure 4(b) shows the  $k^q$  values of the LSCF<sub>113</sub> with double-layer decoration of stacked LSC<sub>214</sub> and three different Sr

contents of LSC<sub>113</sub> (LSC82<sub>113</sub>, LSC64<sub>113</sub>, and LSC46<sub>113</sub>) thin films, extracted from the EIS data [Fig. 4(a)]. As shown in Fig. 4(b), the  $k^q$  values of the LSCF<sub>113</sub> thin films were found to change with the additional LSC<sub>113</sub> phase between the LSCF<sub>113</sub> and LSC<sub>214</sub>, which can be attributed to a change in the Sr concentration at the multiphase heterostructured interface. We hypothesize that the added LSC<sub>113</sub> phase provides sufficient Sr sources for surface Sr redistribution between LSC<sub>113</sub> and LSC<sub>214</sub>, which results in increased Sr segregation on the LSCF interface layer. This hypothesis is consistent with our previous ab initio DFT calculations,<sup>[17]</sup> which found that the thermodynamic driving force for Sr interdiffusion from La<sub>0.625</sub>Sr<sub>0.375</sub>Co<sub>0.25</sub>Fe<sub>0.75</sub>O<sub>3</sub> to (La<sub>0.5</sub>Sr<sub>0.5</sub>)<sub>2</sub>CoO<sub>4</sub> ( $-0.12$  eV) is much weaker than that from La<sub>0.75</sub>Sr<sub>0.25</sub>CoO<sub>3</sub> to (La<sub>0.5</sub>Sr<sub>0.5</sub>)<sub>2</sub>CoO<sub>4</sub> ( $-0.7$  eV). This driving force is likely responsible for different enhancements in the surface Sr content in the LSCF<sub>113</sub> films upon LSC<sub>214</sub> decoration, resulting in different surface exchange kinetics.

LSCF<sub>113</sub> with the double-layer decoration of stacked LSC<sub>214</sub> and LSC46<sub>113</sub> shows significantly higher  $k^q$  values up to  $\sim 1.5$  orders of magnitude relative to the undecorated LSCF<sub>113</sub> and LSC<sub>214</sub>-decorated LSCF<sub>113</sub>. The enhancement can be attributed to Sr segregation at the interface between LSC<sub>214</sub> and LSC46<sub>113</sub> and on the LSC<sub>214</sub> surface at the expense of Sr in LSC46<sub>113</sub> in the double-layer decoration considering markedly enhanced activity of LSC<sub>214</sub>-decorated LSC82<sub>113</sub> in the previous work.<sup>[17]</sup>

In conclusion, we demonstrate that the oxygen surface exchange kinetics of the (001)-oriented epitaxial LSCF<sub>113</sub> thin films can be markedly improved by the advanced heterostructured oxide interface engineering using the single-layer



**Figure 4.** EIS results of microelectrodes (200  $\mu\text{m}$  in diameter) for the epitaxial LSCF<sub>113</sub> thin films with LSC<sub>214</sub> decoration, and double-layer decorations of stacked LSC<sub>214</sub> and LSC<sub>113</sub> on YSZ (001) with a GDC buffer layer at 550 °C. (a) Nyquist plot at 550 °C with an 1 atm of  $p(\text{O}_2)$  of the LSCF<sub>113</sub> (green), the LSC<sub>214</sub>-decorated LSCF<sub>113</sub> (yellow), and the LSCF<sub>113</sub> with double-layer decoration of stacked  $\sim 3$  nm LSC<sub>214</sub> and  $\sim 0.5$  nm LSC82<sub>113</sub> (blue),  $\sim 0.5$  nm LSC64<sub>113</sub> (orange), and  $\sim 0.5$  nm LSC46<sub>113</sub> (red) thin films. (b)  $p(\text{O}_2)$  of the  $k^a$  calculated from EIS spectra collected at 550 °C of the LSCF<sub>113</sub> (green), the LSC<sub>214</sub>-decorated LSCF<sub>113</sub> (yellow), and the LSCF<sub>113</sub> with double-layer decoration of stacked  $\sim 3$  nm LSC<sub>214</sub> and  $\sim 0.5$  nm LSC82<sub>113</sub> (blue),  $\sim 0.5$  nm LSC64<sub>113</sub> (orange), and  $\sim 0.5$  nm LSC46<sub>113</sub> (red) thin films. Inset shows a hypothetical model: enhancement of the Sr content at the interface between the LSCF<sub>113</sub> and the LSC<sub>214</sub> phase due to an increase in the Sr interdiffusion from LSC<sub>113</sub> to LSC<sub>214</sub>.

decoration of mixed LSC<sub>214</sub> and LSC<sub>113</sub> and double-layer decoration of stacked LSC<sub>214</sub> and LSC<sub>113</sub>. This result extends previous results,<sup>[17]</sup> showing enhancement from decoration of LSC<sub>214</sub> on LSC<sub>113</sub> to the LSCF<sub>113</sub> material, which is of significantly more interest for commercial applications than LSC<sub>113</sub>. The oxygen surface exchange coefficients of the LSCF<sub>113</sub> with single-layer decoration of mixed LSC<sub>214</sub> and LSC<sub>113</sub> are  $\sim 1.1$  orders of magnitude greater than those of the undecorated LSCF<sub>113</sub> and LSC<sub>214</sub>-decorated LSCF<sub>113</sub>. In addition, the oxygen surface exchange coefficients of the LSCF<sub>113</sub> with double layer decoration of stacked LSC<sub>214</sub> and LSC<sub>113</sub> are  $\sim 1.5$  orders of magnitude higher than those of the undecorated LSCF<sub>113</sub> with and without LSC<sub>214</sub> decoration. The previous work<sup>[17]</sup> suggests a strong correlation between the O 2*p* band center and surface exchange kinetics, where surface Sr segregation in the perovskite structure and associated O 2*p* band uplift could increase the surface exchange rate. Therefore, we hypothesize that the decoration on the surface of LSCF<sub>113</sub> provides Sr segregation at the interface LSC<sub>214</sub> and LSC<sub>113</sub> and on the surface of LSC<sub>214</sub>, which can uplift in the position of the O 2*p* band center relative to Fermi energy of the LSCF interface layer in comparison to that of the LSCF<sub>113</sub> surface. This work illustrates that heterostructured oxide interface engineering is a strategy, which can enhance multiple types of active oxide materials. Such approaches could potentially be utilized in the infiltration process for decorating cathodes to enhance the performance of SOFCs.

### Supplementary material

The supplementary material for this article can be found at <http://dx.doi.org/10.1557/mrc.2016.28>

### Acknowledgments

This work was supported by the Department of Energy (DOE), National Energy Technology Laboratory (NETL), Solid State Energy Conversion Alliance (SECA) Core Technology Program (Funding Opportunity Number DEFE0009435) and the Skoltech-MIT Center for Electrochemical Energy. The PLD and XRD performed were conducted at the Center for Nanophase Materials Sciences, which is sponsored at Oak Ridge National Laboratory by the Scientific User Facilities Division, Office of Basic Energy Sciences, U.S. Department of Energy, and computations in this work were also benefited from the use of the National Energy Research Scientific Computing Center allocation of the Center for Nanophase Materials Sciences at Oak Ridge National Laboratory, both under grant number CNMS2013-292.

### References

1. Z.P. Shao and S.M. Haile: A high-performance cathode for the next generation of solid-oxide fuel cells. *Nature* **431**, 170 (2004).
2. B.C.H. Steele and A. Heinzel: Materials for fuel-cell technologies. *Nature* **414**, 345 (2001).
3. L. da Conceicao, C.R.B. Silva, N.F.P. Ribeiro, and M. Souza: Influence of the synthesis method on the porosity, microstructure and electrical properties of La<sub>0.7</sub>Sr<sub>0.3</sub>MnO<sub>3</sub> cathode materials. *Mater. Charact.* **60**, 1417 (2009).
4. A. Endo, M. Ihara, H. Komiyama, and K. Yamada: Cathodic reaction mechanism for dense Sr-doped lanthanum manganite electrodes. *Solid State Ion.* **86–88**, 1191 (1996).
5. T. Ioroi, T. Hara, Y. Uchimoto, Z. Ogumi, and Z. Takehara: Preparation of perovskite-type La<sub>1-x</sub>Sr<sub>x</sub>MnO<sub>3</sub> films by vapor-phase processes and their electrochemical properties. *J. Electrochem. Soc.* **144**, 1362 (1997).
6. S.B. Adler: Factors governing oxygen reduction in solid oxide fuel cell cathodes. *Chem. Rev.* **104**, 4791 (2004).

7. S. Wang, M. Katsuki, M. Dokiya, and T. Hashimoto: High temperature properties of  $\text{La}_{0.6}\text{Sr}_{0.4}\text{Co}_{0.8}\text{Fe}_{0.2}\text{O}_{3-\delta}$  phase structure and electrical conductivity. *Solid State Ion.* **159**, 71 (2003).
8. M. Katsuki, S. Wang, M. Dokiya, and T. Hashimoto: High temperature properties of  $\text{La}_{0.6}\text{Sr}_{0.4}\text{Co}_{0.8}\text{Fe}_{0.2}\text{O}_{3-\delta}$  oxygen nonstoichiometry and chemical diffusion constant. *Solid State Ion.* **156**, 453 (2003).
9. M.F. Liu, D. Ding, K. Blinn, X.X. Li, L.F. Nie, and M. Liu: Enhanced performance of LSCF cathode through surface modification. *Int. J. Hydrog. Energy* **37**, 8613 (2012).
10. X.Y. Lou, S.Z. Wang, Z. Liu, L. Yang, and M.L. Liu: Improving  $\text{La}_{0.6}\text{Sr}_{0.4}\text{Co}_{0.2}\text{Fe}_{0.8}\text{O}_{3-\delta}$  cathode performance by infiltration of a  $\text{Sm}_{0.5}\text{Sr}_{0.5}\text{CoO}_{3-\delta}$  coating. *Solid State Ion.* **180**, 1285 (2009).
11. M.E. Lynch, L. Yang, W.T. Qin, J.J. Choi, M.F. Liu, K. Blinn, and M.L. Liu: Enhancement of  $\text{La}_{0.6}\text{Sr}_{0.4}\text{Co}_{0.2}\text{Fe}_{0.8}\text{O}_{3-\delta}$  durability and surface electrocatalytic activity by  $\text{La}_{0.85}\text{Sr}_{0.15}\text{MnO}_{3\pm\delta}$  investigated using a new test electrode platform. *Energy Environ. Sci.* **4**, 2249 (2011).
12. X.B. Zhu, D. Ding, Y.Q. Li, Z. Lu, W.H. Su, and L. Zhen: Development of  $\text{La}_{0.6}\text{Sr}_{0.4}\text{Co}_{0.2}\text{Fe}_{0.8}\text{O}_{3-\delta}$  cathode with an improved stability via  $\text{La}_{0.8}\text{Sr}_{0.2}\text{MnO}_{3-\delta}$  film impregnation. *Int. J. Hydrog. Energy* **38**, 5375 (2013).
13. E.J. Crumlin, S.J. Ahn, D. Lee, E. Mutoro, M.D. Biegalski, H.M. Christen, and Y. Shao-Horn: Oxygen electrocatalysis on epitaxial  $\text{La}_{0.6}\text{Sr}_{0.4}\text{CoO}_{3-\delta}$  perovskite thin films for solid oxide fuel cells. *J. Electrochem. Soc.* **159**, F219 (2012).
14. Z. Feng, E.J. Crumlin, W.T. Hong, D. Lee, E. Mutoro, M.D. Biegalski, H. Zhou, H. Bluhm, H.M. Christen, and Y. Shao-Horn: In situ studies of the temperature-dependent surface structure and chemistry of single-crystalline (001)-oriented  $\text{La}_{0.8}\text{Sr}_{0.2}\text{CoO}_{3-\delta}$  perovskite thin films. *J. Phys. Chem. Lett.* **4**, 1512 (2013).
15. M.J. Gadre, Y.L. Lee, and D. Morgan: Cation interdiffusion model for enhanced oxygen kinetics at oxide heterostructure interfaces. *Phys. Chem. Chem. Phys.* **14**, 2606 (2012).
16. D. Lee, Y.-L. Lee, A. Grimaud, W.T. Hong, M.D. Biegalski, D. Morgan, and Y. Shao-Horn: Enhanced oxygen surface exchange kinetics and stability on epitaxial  $\text{La}_{0.8}\text{Sr}_{0.2}\text{CoO}_{3-\delta}$  thin films by  $\text{La}_{0.8}\text{Sr}_{0.2}\text{MnO}_{3-\delta}$  decoration. *J. Phys. Chem. C* **118**, 14326 (2014).
17. D. Lee, Y.-L. Lee, W.T. Hong, M.D. Biegalski, D. Morgan, and Y. Shao-Horn: Oxygen surface exchange kinetics and stability of  $(\text{La}, \text{Sr})_2\text{CoO}_{4\pm\delta}/\text{La}_{1-x}\text{Sr}_x\text{MO}_{3-\delta}$  ( $\text{M} = \text{Co}$  and  $\text{Fe}$ ) hetero-interfaces at intermediate temperatures. *J. Mater. Chem. A* **3**, 2144 (2015).
18. M. Sase, F. Hermes, K. Yashiro, K. Sato, J. Mizusaki, T. Kawada, N. Sakai, and H. Yokokawa: Enhancement of oxygen surface exchange at the hetero-interface of  $(\text{La}, \text{Sr})\text{CoO}_3/(\text{La}, \text{Sr})_{(2)}\text{CoO}_4$  with PLD-layered films. *J. Electrochem. Soc.* **155**, B793 (2008).
19. E.J. Crumlin, E. Mutoro, S.J. Ahn, G.J. Ia O, D.N. Leonard, A. Borisevich, M.D. Biegalski, H.M. Christen, and Y. Shao-Horn: Oxygen reduction kinetics enhancement on a heterostructured oxide surface for solid oxide fuel cells. *J. Phys. Chem. Lett.* **1**, 3149 (2010).
20. Z.X. Feng, Y. Yacoby, M.J. Gadre, Y.L. Lee, W.T. Hong, H. Zhou, M. D. Biegalski, H.M. Christen, S.B. Adler, D. Morgan, and Y. Shao-Horn: anomalous interface and surface strontium segregation in  $(\text{La}_{1-y}\text{Sr}_y)_2\text{CoO}_{4\pm\delta}/\text{La}_{1-x}\text{Sr}_x\text{CoO}_{3-\delta}$  heterostructured thin films. *J. Phys. Chem. Lett.* **5**, 1027 (2014).
21. T. Nitadori, M. Muramatsu, and M. Misono: Valence control, reactivity of oxygen, and catalytic activity of lanthanum strontium cobalt oxide  $(\text{La}_{2-x}\text{Sr}_x\text{CoO}_4)$ . *Chem. Mater.* **1**, 215 (1989).
22. M. Sase, F. Hermes, T. Nakamura, K. Yashiro, K. Sato, J. Mizusaki, T. Kawada, N. Sakai, K. Yamaji, T. Horita, and H. Yokokawa: Promotion of oxygen surface reaction at the hetero-interface of  $(\text{La}, \text{Sr})\text{CoO}_{(3)}/(\text{La}, \text{Sr})_{(2)}\text{CoO}_{(4)}$ . In *Solid Oxide Fuel Cells 10*, edited by K. Eguchi, S. C. Singhai, H. Yokokawa, and H. Mizusaki (Electrochemical Society Inc, Pennington, 2007), pp. 1055.
23. S. Shinomori, M. Kawasaki, and Y. Tokura: Orientation-controlled epitaxy and anisotropic properties of  $\text{La}_{2-x}\text{Sr}_x\text{NiO}_4$  with  $0.5 \leq x \leq 1.5$  covering the insulator-metal transition. *Appl. Phys. Lett.* **80**, 574 (2002).
24. D. Lee, A. Grimaud, E.J. Crumlin, K. Mezghani, M.A. Habib, Z.X. Feng, W. T. Hong, M.D. Biegalski, H.M. Christen, and Y. Shao-Horn: Strain influence on the oxygen electrocatalysis of the (100)-oriented epitaxial  $\text{La}_2\text{NiO}_{4\pm\delta}$  thin films at elevated temperatures. *J. Phys. Chem. C* **117**, 18789 (2013).
25. D. Lee, Y.-L. Lee, A. Grimaud, W.T. Hong, M.D. Biegalski, D. Morgan, and Y. Shao-Horn: Strontium influence on the oxygen electrocatalysis of  $\text{La}_{2-x}\text{Sr}_x\text{NiO}_{4\pm\delta}$  ( $0.0 \leq x_{\text{Sr}} \leq 1.0$ ) thin films. *J. Mater. Chem. A* **2**, 6480 (2014).
26. M. James, A. Tedesco, D. Cassidy, M. Colella, and P.J. Smythe: The phase diagram and crystal chemistry of strontium-doped rare earth cobaltates:  $\text{Ln}_{(2-x)}\text{Sr}_x\text{CoO}_{(4\pm\delta)}$  ( $\text{Ln} = \text{La-Dy}$ ). *J. Alloys Compd.* **419**, 201 (2006).
27. L.W. Tai, M.M. Nasrallah, H.U. Anderson, D.M. Sparlin, and S.R. Sehlin: Structure and electrical-properties of  $\text{La}_{1-x}\text{Sr}_x\text{Co}_{1-y}\text{Fe}_y\text{O}_{3-\delta}$ . 1. The system  $\text{La}_{0.8}\text{Sr}_{0.2}\text{Co}_{1-y}\text{Fe}_y\text{O}_3$ . *Solid State Ion.* **76**, 259 (1995).
28. R.H.E. van Doorn, and A.J. Burggraaf: Structural aspects of the ionic conductivity of  $\text{La}_{1-x}\text{Sr}_x\text{CoO}_{3-\delta}$ . *Solid State Ion.* **128**, 65 (2000).
29. B.C.H. Steele and J.M. Bae: Properties of  $\text{La}_{0.6}\text{Sr}_{0.4}\text{Co}_{0.2}\text{Fe}_{0.8}\text{O}_{3-\delta}$  (LSCF) double layer cathodes on gadolinium-doped cerium oxide (CGO) electrolytes—II. Role of oxygen exchange and diffusion. *Solid State Ion.* **106**, 255 (1998).
30. Y.L. Lee, J. Kleis, J. Rossmel, Y. Shao-Horn, and D. Morgan: Prediction of solid oxide fuel cell cathode activity with first-principles descriptors. *Energy Environ. Sci.* **4**, 3966 (2011).